Supplementary material

Energetically Quasi-Integrable Roaming in the Ionized CH_4 + CO System: Nonequilibrium Dynamics of Acetaldehyde Formation

Toshiaki Matsubara*

Department of Chemistry, Faculty of Science, Kanagawa University,
3-27-1, Rokkakubashi, Kanagawa-ku, Yokohama 221-8686, Japan

1. **Note S1.** NBO charges, overlap integrals, and bond populations
2. **Note S2.** Sequential $CH_3\cdots HCO^+$ and $CH_4^+\cdots CO$ roaming dynamics
3. **Fig. S3.** Relative translational kinetic energy
4. **Fig. S4.** Scatter plot of the C–C distance versus the relative translational kinetic energy
5. Cartesian coordinates of the optimized structures.

Note S1. NBO charges, overlap integrals, and bond populations.

Fig. S1 presents the time evolution of electronic descriptors along a representative MD trajectory leading to CH_3CHO^+ formation. Panels (a) and (b) show the NBO charges of the relevant fragments during the $CH_4^+\cdots CO$ roaming regime and the subsequent $CH_3\cdots HCO^+$ roaming regime, respectively. During the $CH_4^+\cdots CO$ roaming stage, the charge distribution remains largely localized on the CH_4^+ fragment, with only minor charge fluctuations on both fragments. In contrast, during the $CH_3\cdots HCO^+$ roaming stage, the charge distribution becomes significantly localized on the HCO^+ fragment, exhibiting noticeable changes as the hydrogen atom approaches the CO fragment.

Panel (c) shows the time-dependent overlap integral between carbon-centered orbitals. The overlap remains negligible during the $CH_4^+\cdots CO$ roaming regime but increases intermittently during the $CH_3\cdots HCO^+$ roaming stage, indicating repeated transient C–C orbital interactions. Panel (d) displays the corresponding C–C bond population. During the $CH_4^+\cdots CO$ roaming regime, the bond population remains close to zero, whereas during the $CH_3\cdots HCO^+$ roaming regime it exhibits pronounced fluctuations, reflecting intermittent changes in the C–C electronic interaction as the two carbon centers approach each other along the roaming trajectory.

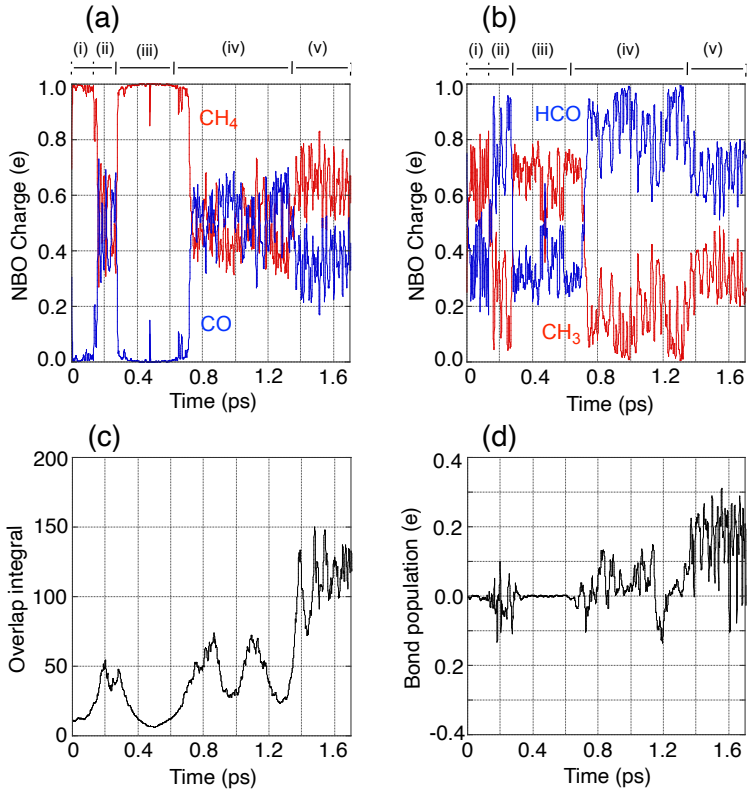

Fig. S1 Time evolution of electronic structure descriptors along a representative MD trajectory leading to CH_3CHO^+ formation during the $CH_4^+\cdots CO$ roaming regime and the subsequent $CH_3\cdots HCO^+$ roaming regime. Panels (a) and (b) show the NBO charges of the fragments, panel (c) shows the overlap integral between carbon-centered orbitals associated with the C–C interaction, and panel (d) shows the corresponding C–C bond population.

Note S2. Sequential $CH_3\cdots HCO^+$ and $CH_4^+\cdots CO$ roaming dynamics.

Fig. S2 presents a representative trajectory illustrating post-formation roaming dynamics following the initial formation of CH_3CHO^+. In this analysis, we focus exclusively on the roaming segments that occur after the first formation of CH_3CHO^+; the final dissociation into $CH_3 + CHO^+$, although observed in the trajectory, is not discussed in detail here. Following the exothermic formation of CH_3CHO^+, the system enters an initial $CH_3\cdots HCO^+$ roaming regime in region (i), which is followed by re-formation of CH_3CHO^+ in region (ii) (panel (a)). The system then re-enters a second $CH_3\cdots HCO^+$ roaming regime in region (iii). During this stage, both fragments exhibit large-amplitude translational motion; nevertheless, dissociation does not occur, and the fragments remain dynamically correlated throughout the roaming motion. Notably, in the $CH_3\cdots HCO^+$ roaming regimes observed after CH_3CHO^+ formation, kinetic energy is redistributed toward the HCO^+ fragment through H-atom motion within CH_3CHO^+ (panel (b)). Despite this redistribution, the system remains in an energetically decoupled roaming state, and dissociation does not occur.

Subsequently, the system evolves into a $CH_4^+\cdots CO$ roaming regime in region (iv) (panel (a)), representing a qualitatively different roaming regime. This transition is accompanied by a pronounced redistribution of kinetic energy between the fragments, where the kinetic energy of the CO fragment becomes strongly suppressed (panel (b)), remaining small and nearly constant. As a result, the fragments exhibit slow roaming motion, characteristic of a dynamically stabilized roaming state.

To further characterize the nature of the two roaming regimes, we analyzed the energetic behavior and electronic coupling between the fragments in both the $CH_3\cdots HCO^+$ and $CH_4^+\cdots CO$ roaming states. In both regimes, the sum of potential and kinetic energies (PE + KE) of each fragment remains nearly constant over time (panel (c) and (d)), indicating limited energy exchange between the fragments. Consistently, the overlap integrals (panel (e)) and bond populations (panel (f)) between the fragments are small and remain nearly constant throughout the roaming periods, reflecting weak electronic coupling. These results indicate that both roaming regimes correspond to transiently energetically decoupled, quasi-integrable fragment motions.

Analysis of the interaction energy (panels (g) and (h)) reveals distinct correlations in the two roaming regimes. In the $CH_3\cdots HCO^+$ roaming regime, the temporal variation of the interaction energy closely follows the energy fluctuations of the HCO^+ fragment, whereas in the $CH_4^+\cdots CO$ roaming regime, it correlates with the energy fluctuations of the CH_4^+ fragment. This indicates that, in the $CH_3\cdots HCO^+$ roaming regime, the strength of the interfragment interaction is primarily governed by the energy of the HCO^+ fragment rather than that of the CH_3 fragment, suggesting that the HCO^+ fragment acts as the primary mediator of the residual interfragment coupling. In contrast, in the $CH_4^+\cdots CO$ roaming regime, the interfragment interaction is predominantly controlled by the energy of the CH_4^+ fragment rather than that of the CO fragment. These marginal energetic couplings between the fragments provide a plausible physical basis for the persistence of the long-lived roaming motion.

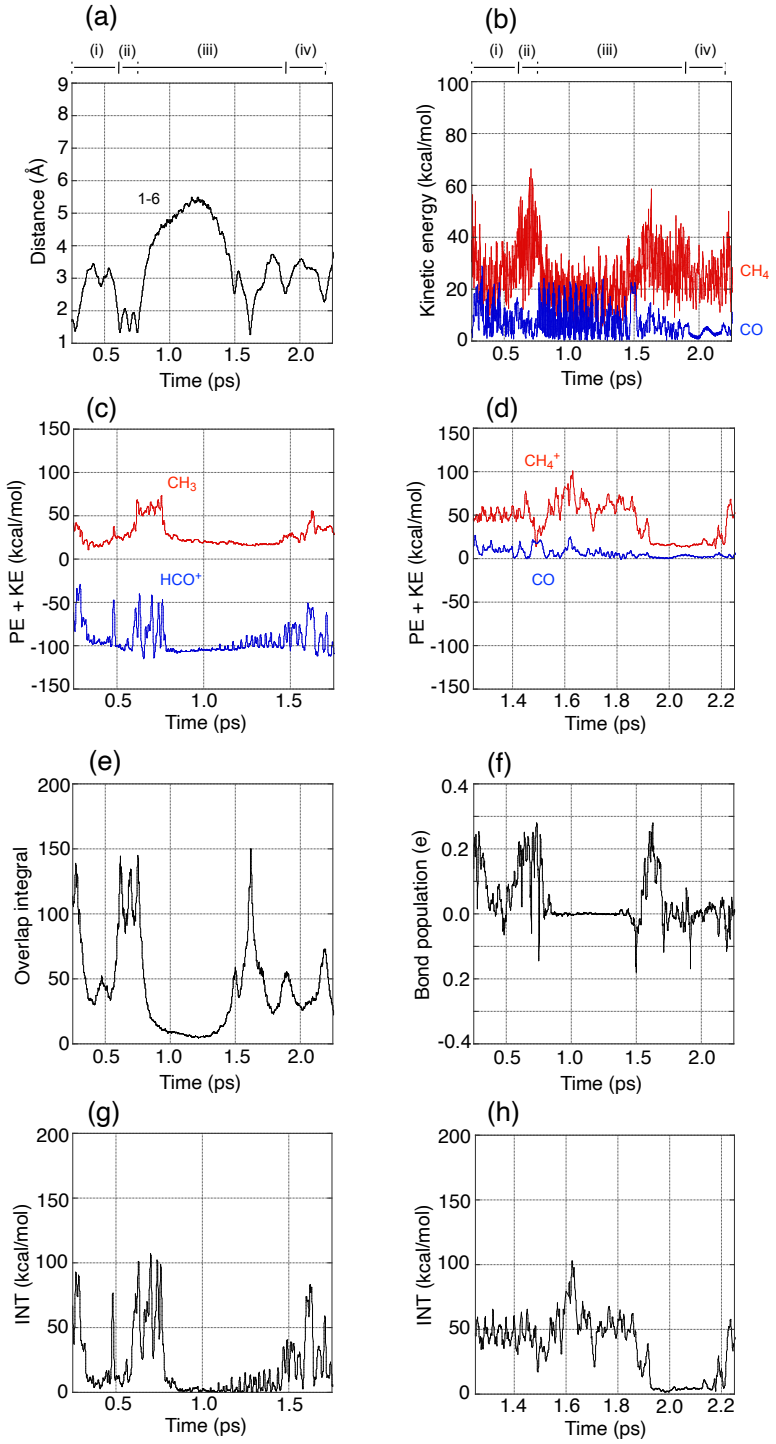

Fig. S2 Time evolution of a representative trajectory showing sequential $CH_3\cdots HCO^+$ and $CH_4^+\cdots CO$ roaming following the initial formation of CH_3CHO^+. Panel (a) shows the C^1–C^6 distance; panel (b) shows the kinetic energy of each fragment; panels (c) and (d) show the sum of potential and kinetic energies (PE + KE) for each fragment; panel (e) shows the overlap integral between carbon-centered orbitals associated with the C–C interaction; panel (f) shows the corresponding C–C bond population; panels (g) and (h) show the interaction energies (INT) for the $CH_3\cdots HCO^+$ and $CH_4^+\cdots CO$ pairs, respectively. $CH_3\cdots HCO^+$ roaming first occurs in region (i), followed by re-formation of CH_3CHO^+

in region (ii). In region (iii), $CH_3\cdots HCO^+$ roaming occurs twice, with transient re-formation of CH_3CHO^+ along the pathway. In region (iv), $CH_4^+\cdots CO$ roaming is observed.

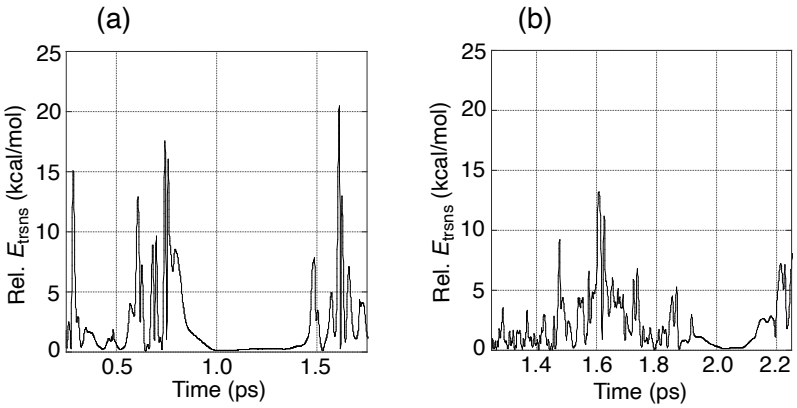

Fig. S3 Relative translational kinetic energy between (a) CH_3 and HCO and (b) CH_4 and CO as functions of time along the representative trajectory presented in Fig. S2.

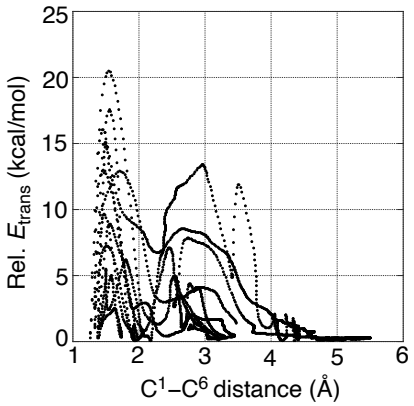

Fig. S4 Relation between the interfragment C^1–C^6 distance and the relative translational kinetic energy Rel. E_{trans} for the representative $CH_3\cdots HCO$ roaming trajectory presented in Fig. S2. The data points correspond to time steps belonging to the large-amplitude roaming excursion. As in the $CH_4\cdots CO$ roaming case, the relative translational kinetic energy approaches near-zero values at large separations, consistent with transient dynamical decoupling between the fragments.

Cartesian coordinates (in Å)

1

C -2.918114 0.024130 0.000020
H -3.840026 -0.419961 -0.367029
H -3.115801 0.551894 0.929648
H -2.533578 0.723293 -0.738411
H -2.181689 -0.755731 0.175067
C 1.472330 -0.207679 0.000447
O 2.543225 0.125225 -0.000259

2

C 2.084349 -0.000199 0.000066
H 2.220574 -0.738101 0.782057
H 2.213007 -0.311943 -1.029984
H 2.226541 1.045801 0.244731
H 0.478425 0.002317 0.000662
C -0.773270 0.001218 0.000107
O -1.875628 -0.000523 0.000187

3

C 1.172992 -0.150318 -0.000003
H 1.162747 -1.234954 -0.000311
H 1.651296 0.270276 -0.889701
H 1.651003 0.269767 0.890082
C -0.233950 0.395551 -0.000006
O -1.212318 -0.284363 -0.000000
H -0.400750 1.498420 -0.000015

5

C -0.219138 0.000181 0.000121
O -1.325804 -0.000063 -0.000025
C 1.212991 -0.000037 -0.000077
H 1.547377 -0.892739 -0.538169
H 1.547821 0.912378 -0.503747
H 1.548117 -0.020000 1.041854

7

C 0.029767 0.459022 -0.000040
C -1.213336 -0.199217 -0.000018
H -2.122307 0.385852 -0.000232
H -1.278202 -1.280798 0.000412
H 0.108470 1.541808 0.000282
O 1.158600 -0.136696 0.000019
H 1.124651 -1.112117 -0.000262

8

C -1.228838 -0.175325 0.000019
C 0.030727 0.442468 0.000014
H -1.295636 -1.255707 -0.000072
H -2.123605 0.430231 -0.000212
H 0.148886 1.522916 0.000121
O 1.067516 -0.308286 0.000052
H 1.918887 0.165992 -0.000450

9

C -1.234672 -0.093825 -0.000054
C 0.115826 0.408735 -0.000047
O 1.180795 -0.209682 0.000002
H 2.006615 0.323977 0.000049
H -1.744716 0.326516 -0.874961
H -1.743132 0.323175 0.877375
H -1.252054 -1.185678 -0.001869

TS1

C -1.919517 -0.128368 -0.000478
H -2.374464 0.851706 0.071820
H -1.867912 -0.609005 -0.967503
H -1.843071 -0.732016 0.892962
O 1.616368 -0.303037 0.000071
C 0.798404 0.438545 0.000597
H -0.118820 1.052548 0.001438

TS2

C -0.217576 0.593226 -0.000177
C 1.071500 -0.097449 0.000029
O -0.981401 -0.387060 0.000114
H -0.576486 1.621066 -0.000110
H 1.598827 -0.181022 0.948783
H 1.597834 -0.182722 -0.949141
H 0.107490 -1.135508 0.000439

TS3

C 0.011840 0.457840 0.016635
C -1.225206 -0.216662 0.008829
H -2.145548 0.348001 0.082017
H -1.252058 -1.296222 -0.075921
H 0.058941 1.546177 0.017082
O 1.117787 -0.187001 -0.098128
H 1.676561 -0.549018 0.609056

TS4

C 1.232351 -0.154900 0.027201
C -0.030024 0.350228 0.119799
H 2.064888 0.468136 0.339018
H 1.411844 -1.142906 -0.401524
H 0.589422 0.876280 -0.816202
O -1.171203 -0.217289 0.027410
H -1.910489 0.364838 -0.222573

TS5

C 1.245963 0.076104 0.000004
C -0.156883 -0.298916 -0.000111
O -1.251537 0.237677 0.000013
H 1.326536 1.166013 -0.000445
H 1.712603 -0.371624 0.883576
H 1.713204 -0.372501 -0.882785
H -1.274533 -0.986436 0.000189